Nuclear Instruments and Methods in Physics Research A 391 (1997) 485–491

NUCLEAR INSTRUMENTS & METHODS IN PHYSICS RESEARCH Section A

ELSEVIER

Neutron diffraction from sound-excited crystals

A. Remhof[a], K.-D. Liß[b], A. Magerl[c,*]

[a] *Ruhruniversität Bochum, D-44780 Bochum, Germany*
[b] *European Synchrotron Radiation Facility, F-38043 Grenoble Cedex 9, France*
[c] *Institut Max von Laue–Paul Langevin, F-38042 Grenoble, France*

Received 20 November 1996; revised form received 11 February 1997

Abstract

A longitudinal sound wave modulates the regular arrangement of the atomic planes of a crystal in two ways: first, the spacing between the atomic planes is modified in the regions of compression and expansion introducing a macroscopic strain and, second, the lattice planes acquire a velocity in the oscillating strain field. Bragg reflection in a strained crystal maintains the energy of the radiation, whereas Bragg reflection by a moving lattice provokes a Doppler shift of the radiation. In a diffraction experiment both these effects lead to an enlarged bandwidth of the reflection curve. The relative importance of strain and Doppler depends mainly on the radiation used. For thermal neutron scattering the profile of the rocking curve of a Bragg reflection may permit to separate the two effects. Atomic amplitudes of the sound field of 136 Å peak to peak in the bulk of the crystal can be deduced from the rocking profile. The enlarged bandwidth of a sound-excited crystal opens a possibility for diffraction-based optical elements where the trade-off between resolution and intensity can be readily modified.

PACS: 61.12; 63.20.-e; 03.75.B
Keywords: Diffraction; Solid state dynamics; Ultrasound; Neutron optics

1. Introduction

Exciting a longitudinal sound wave in a crystal causes an oscillatory modulation of the lattice parameter in space and time. For a standing wave the positions of the antinodes are stationary whereas the amplitude changes with the sound frequency. These modulations vary the lattice parameter introducing strain- and Doppler gradients. In analogy to a mosaic crystal [1], the diffraction behaviour of a vibrating crystal can be understood assuming that it consists of small volume elements with a perfect structure. Within each of these strain blocks, there is a well-defined value for the lattice spacing with a negligible gradient. Similarly, the crystal may be broken up into velocity blocks, where all the lattice planes within a block have the same velocity. The sizes of the strain blocks and the velocity blocks may be different. They depend on the material and the reflection used, on the amplitude and the frequency of the sound wave, and on the particle velocity of the radiation. In any case, the thickness of the blocks must be chosen such that the variation of the parameter in question within a block is smaller than its variation allowed by the Darwin width from dynamical diffraction [2]. A non-excited crystal will be composed out of one block and its thickness may exceed the extinction length of an ideal crystal. In this case, the diffracted intensity will be limited according to the dynamical theory. At large deformations, both the gradient blocks and the velocity blocks may become thin enough such that primary extinction becomes negligible and the diffracted intensity will approach the kinematical limit.

Unlike mosaic blocks, which are tilted against each other, the surface normals of both the gradient blocks and the velocity blocks are parallel to each other and they are also parallel to the propagation vector of the sound wave. Thus, in case the diffraction vector is also chosen parallel to the propagation vector of the wave as in the present experiment, a sound-excited crystal represents an oscillating gradient crystal. Such crystals are known to have favourable diffraction properties [3,4]. E.g., they maintain the beam divergencies after

* Corresponding author. Tel.: +33 76 207383; fax: +33 76 483906; e-mail: magerl@ill.fr.

PII S0168-9002(97)00411-7

diffraction and they may allow to pile up more intensity in a given direction than it is possible with mosaic crystals.

2. Theory

A one-dimensional longitudinal standing wave with angular frequency ω, wave number k and an atomic amplitude u_0, is described by [5]

$$u(x,t) = u_0 \sin(kx) \sin(\omega t) \tag{1}$$

containing the two variables x and t for space and time, respectively. The partial derivative of Eq. (1) with respect to the spatial variable x

$$\frac{\partial u(x,t)}{\partial x} = u_0 k \cos(kx) \sin(\omega t) \tag{2}$$

describes the strain field which modifies the lattice spacing d according to

$$\left[\frac{\Delta d}{d}\right]_{\text{strain}} = \frac{\partial u(x,t)}{\partial x}. \tag{3}$$

The partial derivative of Eq. (1) with respect to time

$$\frac{\partial u(x,t)}{\partial t} = u_0 \omega \sin(kx) \cos(\omega t) \tag{4}$$

attributes a velocity v_{hkl} to the atomic planes which is chosen here parallel to the propagation vector of the sound. The energy of a radiation Bragg-reflected by these planes becomes Doppler shifted by v_{Doppler}. The relative change of the velocity of the beam diffracted at a Bragg angle θ from a lattice reflection hkl is

$$\frac{v_{hkl}}{v_P} = -\frac{u_0 \omega}{v_P} \sin(kx) \cos(\omega t) \sin(\theta), \tag{5}$$

where v_P is the particle velocity with the diffracting planes at rest. The relative Doppler shift can also be viewed as a modification of the crystal spacing yielding

$$\left[\frac{\Delta d}{d}\right]_{\text{Doppler}} = \frac{v_{hkl}}{v_P}. \tag{6}$$

The total variation of the grating distance d is given by the sum

$$\begin{aligned}\left[\frac{\Delta d}{d}\right]_{\text{tot}} &= \left[\frac{\Delta d}{d}\right]_{\text{strain}} + \left[\frac{\Delta d}{d}\right]_{\text{Doppler}} \\ &= u_0 k \left[\cos(kx) \sin(\omega t) - \frac{v_{\text{sound}} \sin(\theta)}{v_P} \sin(kx) \cos(\omega t)\right].\end{aligned} \tag{7}$$

The strain and Doppler effect are phase shifted by $\pi/2$ in space and time. The lattice planes reach their maximum velocity at the positions of the nodes of the strain when the crystal is unstrained, and they are at rest at the positions of the nodes of the velocity when the strain field is at its peak value.

In the case of thermal neutron diffraction where v_P is of the order of 2000 m/s, and for typical longitudinal sound velocities in solids of 10 000 m/s, the Doppler effect will exceed the contribution from the strain field by a factor $v_{\text{sound}} \sin(\Theta)/v_P$. In contrast, the Doppler effect becomes negligible for X-rays where the speed of light exceeds largely any sound velocity in solids.

Relating to Bragg's law, the width of a rocking curve for monochromatic radiation is given by

$$\Delta\theta = tg(\theta)\frac{\Delta d}{d}. \tag{8}$$

Thus, a measurement of the rocking curve reveals the variations for $\Delta d/d$ and the value of u_0 for the displacement of the diffracting planes can be extracted according to Eqs. (7) and (8).

3. Experimental setup

Longitudinal ultrasonic waves were excited in silicon (Si) and germanium (Ge) crystals by attaching them to piezoelectric lithiumniobate ($LiNbO_3$) transducers with a diameter of 1 in. and a fundamental frequency of 5 MHz. Vacuum grease was used as a viscous coupling medium to suppress transversal modes. The surface normal of the Si and Ge and thus of the propagation vector $\boldsymbol{k}$ of the ultrasonic wave coincides with the [1 1 1] direction. The sound velocities as calculated from the elastic constants [6] are 9360 and 5560 m/s for Si and Ge, respectively.

Since the ultrasonic damping in Si and Ge is low [7], strong mechanic resonances can be observed. They are best identified by bringing the sample in Bragg position and tuning the frequency to the maximum intensity of the diffracted beam.

Two independent experiments have been carried out on the two diffractometers T13 and IN10 at the ILL [8] to make evident the particular diffraction properties relating to the dynamic variation in the lattice vector for sound-excited crystals. T13 is a standard two-axis diffractometer with a layout as shown in Fig. 1(a). A 10 mm thick perfect Si crystal was mounted in a non-dispersive geometry [9] and the evolution of the rocking curve with increasing sound amplitude was followed. The optimum resolution is obtained at the highest take-off angle which, on T13, is limited to 54.5°. For a Si 1 1 1 monochromator this gives a neutron wavelength of 5.1 Å corresponding to a neutron velocity of 782 m/s.

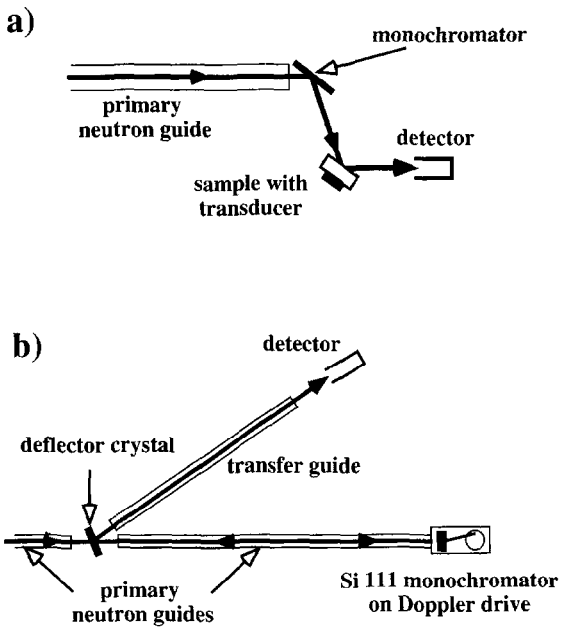

Fig. 1. Layout of the two-axis diffractometer T13 (a) and of the neutron backscattering spectrometer IN10 (b) at the ILL [8].

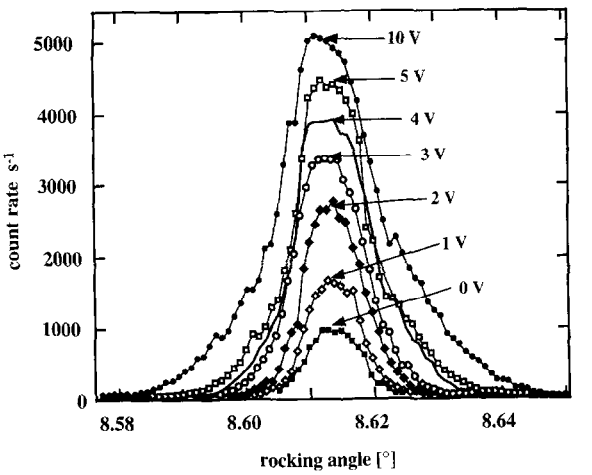

Fig. 2. Si 111 rocking curves measured on T13 for different ultrasonic excitations given by the transducer voltages. The ultrasound frequency is 4.253 MHz.

IN10 shown in Fig. 1(b) is a highly specialised crystal spectrometer in backscattering geometry to achieve best energy resolution. The Doppler-driven Si 1 1 1 monochromator generates a neutron beam centred around an energy $E_0 = 2080\ \mu eV$ and provides an energy scan range of $|\Delta E| = 15\ \mu eV$. The mean energy corresponds to a neutron wavelength of $\lambda = 6.271$ Å or to a neutron velocity of 631 m/s. In the usual setup, the instrument features a deflector crystal made from pyrolythic graphite which deviates the monochromatic neutron beam away from the primary beam into a transfer guide, leading to the sample position. A detector was placed at this location to monitor the incident neutron flux. In the present experiment, the graphite crystal was replaced by a Ge 1 1 1 crystal excited by an ultrasound transducer. This crystal covered only half of the beam cross section.

4. Results and data evaluation

4.1. Measurements on the two-axis diffractometer T13

The rocking width of one perfect Si 1 1 1 crystal at a Bragg angle of 54.5° is 6.1″. (This corresponds to an extinction-limited value $\Delta d/d = 2.1 \times 10^{-5}$). In a non-dispersive two-crystal setup, the total rocking width is given by the convolution of two Darwin curves which is approximately twice the rocking width of a single crystal. Experimentally, a larger width of 43″ is observed. We attribute this increase mainly to a non-ideal quality of the monochromator and, to a lesser extent, also to insufficient precision of the mechanics.

Fig. 2 shows rocking curves for ultrasonic excitations at 4.253 MHz. This corresponds to a resonance with a standing wave pattern comprising $\frac{9}{2}$ wavelengths in the sample. Up to an amplifier voltage of 5 V, the line shape remains largely unchanged, whereas the profile starts to broaden at higher voltage. In particular, there is more pronounced intensity in the lower part of the wings of the spectrum for an excitation of 10 V. The evolution of the integrated intensity with the transducer voltage is displayed in Fig. 3. Over the entire range it increases steadily and a maximum gain factor of about 10 is obtained for the highest transducer voltage. We do not attribute the less than linear increase indicated by the data point for the highest transducer voltage to a saturation of the crystal reflectivity, but to non-linearities of the setup relating, e.g. to heating problems. This demonstrates the potential for applications of sound-excited crystals as neutron-optical elements with tunable intensity.

Fig. 4(a) shows the rocking curves for a perfect crystal and for a crystal excited with a voltage of 45 V at its $\frac{31}{2}\lambda$ resonance at 15.564 MHz. The rocking curve of the excited crystal clearly consists of two components. Correcting for the measured instrumental resolution, the intrinsic full-widths at the base (FWB), which reflect directly the sound amplitude u_0, are 38″ and 429″ for the narrow and the wide component, respectively.

We attribute the narrow and the wide component to the strain field and the Doppler effect, respectively. The ratio of the resolution-corrected widths is 11.3, which compares well with an expected ratio of 10.3 as deduced from Eq. (7). With Eqs. (7) and (8), a strain field of $\Delta d/d = 1.3 \times 10^{-4}$ (full-width) is derived from the narrow

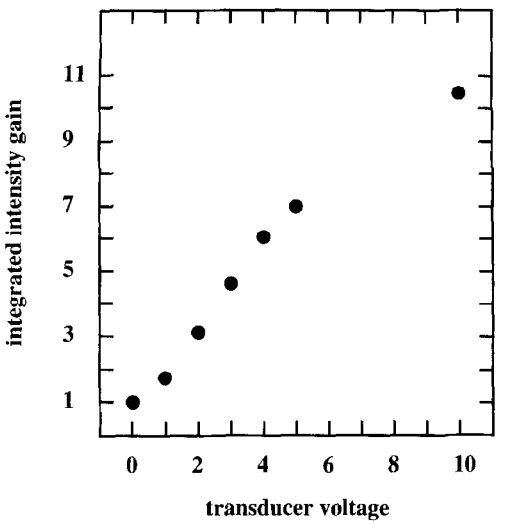

Fig. 3. Gain in integrated intensities from the rocking curves in Fig. 2. The size of the dots represents the error bars.

component and a strain field of $\Delta d/d = 1.5 \times 10^{-4}$ is derived from the wide component. The mean value of $\Delta d/d = 1.4 \times 10^{-4}$ gives an amplitude of motion of the atomic planes of $u_0 = 68$ Å and a maximum value for the lattice velocity of 0.66 m/s.

Addressing the line shape in Fig. 4(a), we note that the diffraction pattern of an ideal crystal is described by the theory of dynamical diffraction [2,10] which assumes perfect phase coherence between all diffracting planes and, moreover, a constant phase shift between these planes relating to the translational symmetry of the crystal. A sound-excited crystal remains perfectly coherent in the sense that all lattice planes have well-defined phase relations. However, the phase shifts are no longer constant, neither in space nor in time, and a description within the dynamical theory of diffraction is no longer appropriate. For standing waves there are moments, when the crystal is completely strain-free and when the Doppler shift vanishes, i.e. all atomic displacements are zero and all atomic displacements are at their maximum value, respectively. These conditions are only fulfilled during a short fraction of an oscillation period. This is so because the Darwin width in Si corresponds to a $\Delta d/d = 2.1 \times 10^{-5}$ whereas the sound excitations yield distortions exceeding the $\Delta d/d$ by a factor of 10 and 100 for the strain field and the Doppler contribution, respectively. As the two effects are phase shifted by $\pi/2$, the crystal never appears to be perfect.

For kinematical scattering, the line shape of a rocking scan represents the density of states for the lattice parameter distribution within the strain field and the density of states for the velocity distribution within the Doppler shift. A sinusoidal standing wave results in similar shape

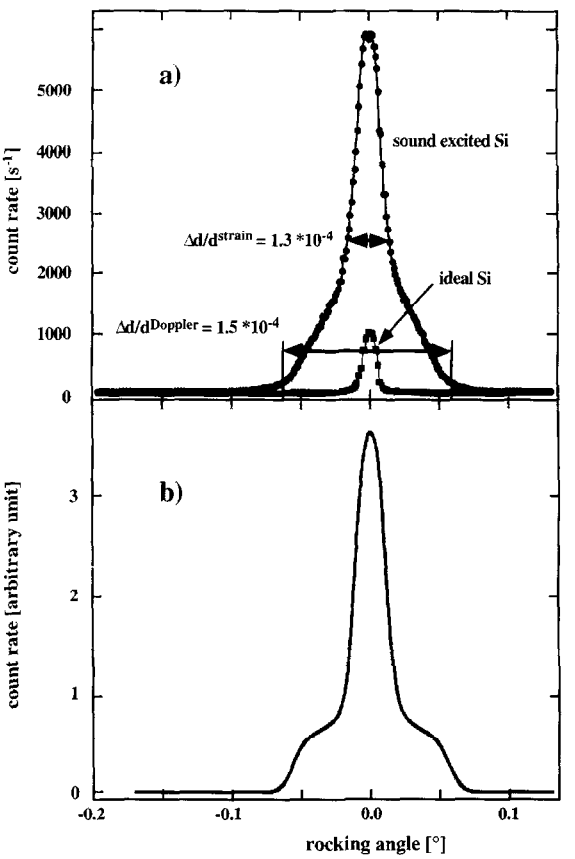

Fig. 4. Panel (a) shows rocking curves for a perfect silicon crystal and for a crystal excited at 15.564 MHz with a transducer voltage of 45 V. The quoted $\Delta d/d$ values are corrected for the instrumental resolution. Panel (b) represents a modelisation of the shape of the rocking curve of a sound-excited crystal within a kinematical approach. The model curve has been convoluted with the instrumental resolution function.

for these two probabilities, which is obtained from an elliptical integral of first order [11]. However, the rocking profiles will extend over a different angular range. Fig. 4(b) shows a description of the experimental data with appropriate density of state functions for strain and Doppler effect, both convoluted with the experimental resolution function obtained from the non-excited crystal. Note that, in addition to an overall scale factor, there is only one adjustable parameter for one rocking width.

4.2. Measurements on the neutron backscattering spectrometer IN10

The upper curve in Fig. 5 shows the neutron spectrum at the sample position of IN10 measured with the usual graphite deflector. The two divergencies found for maximum energy transfers relate to the probability function

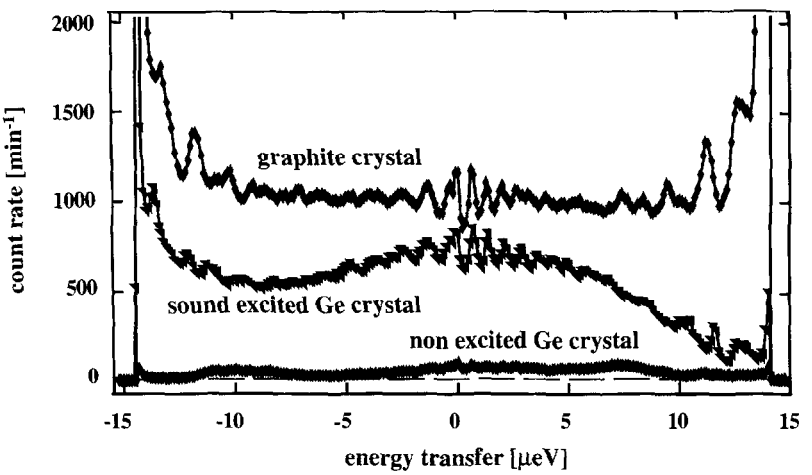

Fig. 5. Neutron spectra at the sample position on IN10 measured with the standard HOPG graphite deflector, with a nearly perfect Ge deflector, and a sound-excited Ge deflector crystal.

of the velocity distribution of the sinusoidal Doppler drive when it is analysed at constant time intervals. This function becomes multiplied by a wavelength-dependent reflectivity curve for the graphite crystal and by the transmission of the neutron guide, which then determines the essential features of the monitor spectrum as observed in Fig. 5. In addition, the data show high-frequency oscillatory features originating from irregularities in the mechanics of the Doppler drive. The spectrum shows further a slight asymmetry indicating a misalignement of the graphite deflector crystal. These two latter features are not of relevance for the following.

Replacing the graphite by a non-excited Ge crystal reduces strongly the intensity of the neutron beam as shown by the lower curve in Fig. 5. Ultra-sound excitation boosts the reflectivity strongly up and the measured data reach about 70% of the intensity of the graphite crystal for zero-energy transfer. The asymmetry of the spectrum points again towards a slight misalignement of the instrument. A more perfect alignement would symmetrise the shape of the spectrum, but it would not increase the integrated beam intensity. It is important to recall at this point that the graphite crystal is big enough to reflect the entire beam, while the Ge crystal covers only half of its size. Taking this into account, it may be postulated as the main result that the flux with a sound-driven Ge deflector exceeds the flux from a graphite-based setup in the central region of the spectrum, whereas it becomes significantly lower at the high-energy region of the spectrum.

Fig. 6 gives a phase-space representation of the reflection conditions at the deflector crystals. All components for beam divergencies and for $\boldsymbol{k}$ vector gradients are multiplied by a factor of 10 for increased clarity whereas angles and wave vectors are drawn to scale. However, the intrinsic line widths for both Si and Ge are too narrow to be shown to scale. This representation allows to appreciate the salient features of the reflection condition. The impinging phase-space element is defined by the perfect Si 111 monochromator in backscattering which has a natural line width of $\Delta d/d = 2.1 \times 10^{-5}$. The $\boldsymbol{k}_i$-value of the phase-space element is modulated by $\pm 0.35\%$ by the mechanical motion of the monochromator. The transverse extension of the phase-space element is given by the angle of total reflection of the Ni-coated guide, which is 38′ at a wavelength of 6.3 Å. The graphite crystal with a mosaicity of some 60′ accepts the major part of the incoming phase-space element and only a small fraction of the neutrons at high-energy transfers located in the corners of the phase-space element will not be reflected. For a complete description of the diffraction process, the out-of-plane beam properties, not represented in Fig. 6, need to be considered as well. The mosaicity of the graphite will increase the vertical divergence of the beam after reflection, and this increased divergence causes a loss of about 50% of the neutrons in the transfer guide.

Replacing the graphite deflector by a Ge crystal (Fig. 6(b)) with a narrow rocking width results first in a dramatic loss in neutron flux at the sample position. For perfect Ge 1 1 1 with $\Delta d/d = 4.0 \times 10^{-5}$, the accepted fraction of the impinging phase-space elements is only 0.7%. Since an ideal crystal reflects like an optical mirror, the vertical beam divergence remains unchanged. Thus, the loss factor discussed above for graphite will not occur and all reflected neutrons will reach the sample position. However, this gain is compensated in the present case by the fact that the Ge covers only about half of the beam size, as already mentioned.

Any crystal imperfection will rapidly enhance the reflecting power of an ideal crystal. Indeed, our Ge is far

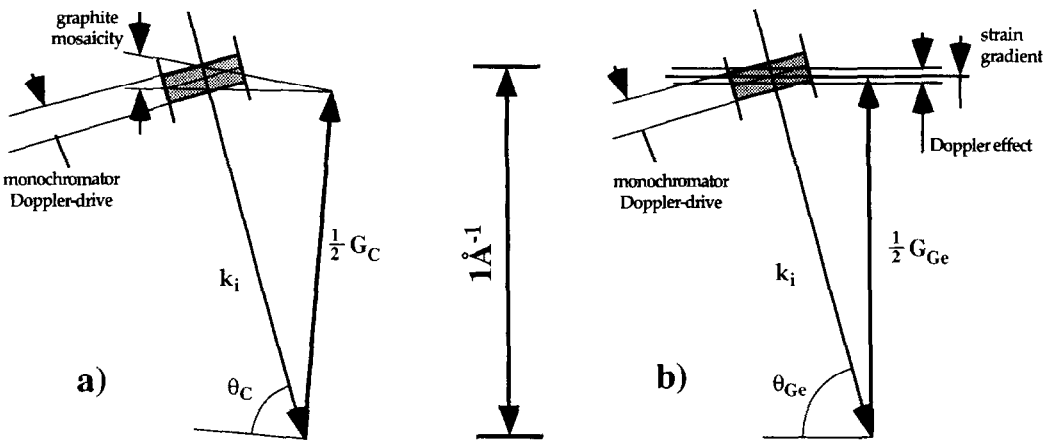

Fig. 6. Phase-space representation of the reflection properties of a graphite crystal (a) and of a sound excited Ge 1 1 1 crystal (b) used as a deflector on IN10.

from perfect, as evidenced by neutron topography [12]. This increases the actual neutron flux at the sample position to 6.5% of the value of the graphite deflector at zero-energy transfer.

Applying an ultrasonic wave with a transducer voltage of 50 V increases the reflection width for the Ge relating to both the strain and the Doppler effect. The reflection widths shown in Fig. 6(b) were extracted from the intensity gains in Fig. 5. Obviously, the dominant effect, in particular for higher-energy transfers, arises from the Doppler effect while strain is only of importance close to the elastic region. The enlarged reflection width of the Ge brings about the strong increase by a factor of 11 of the neutron flux which is reflected towards the sample.

As compared to the graphite deflector, the flux for the sound-excited Ge reaches 75% in the central part of the spectrum. Considering the different crystal sizes, this implies that the sound-excited Ge has better performance than the graphite deflector. This increase in flux relates primarily to the fact that a gradient crystal does not increase the vertical beam divergence. This specific advantage of gradient crystals avoids the transmission losses in the neutron transfer guide and holds promise for a higher flux at the sample position. For high-energy transfer the augmentation of the spectrum is less pronounced. This is understood from Fig. 6(b). It shows clearly that the increase of the reflection width needs to be doubled to have the complete incoming phase-space element accepted by the sound-excited Ge deflector.

At this point it should be noted that, while the experiment on IN10 is well suited to elucidate the diffraction properties of a sound excited crystal, the actual setup as a deflector for a highly monochromatic beam may not be suited for applications. Under such conditions, the deflector becomes an active element which will modify the wavelength of the beam and spoil the energy resolution [16]. However, this disadvantage is very specific to the conditions on IN10, while it will be irrelevant in many other settings.

5. Summary

A longitudinal ultrasound wave introduces both a strain field and a Doppler effect in a crystal. These two modulations of the lattice can be separated by taking rocking scans under favourable conditions. The ratio of the widths of the two components of the rocking curve corresponds to the ratio of the speed of sound of the crystal and the neutron velocity as predicted by theory. The absolute values of the rocking widths allow a direct and precise determination of the atomic amplitudes and of the velocities of the lattice planes which for the highest sound excitations were found to be 136 Å peak to peak and 0.66 m/s, respectively. The shape of the rocking curve reflects the densities of states for the distribution of lattice parameters and for the atomic velocities.

An ultrasound-excited crystal can be understood as an oscillating gradient crystal. Hence, its reflection properties are analogous to an optical mirror, and the Bragg reflected beam maintains the divergencies of the incident beam for both the in-plane and the out-of-plane component. The use of gradient crystals in neutron optics has been discussed earlier [3,4,13–15]. We have addressed the potential of sound-excited gradient crystals as optical elements for particular applications in neutron diffraction. The experiments have demonstrated that, in a high-resolution setup, a sound-driven Ge 1 1 1 may reflect a higher neutron flux towards a sample as it is possible with standard mosaic crystals.

The gradients obtained were small, and hence the integrated intensities were low. In high-resolution experiments, where high reflectivity over a small bandwidth $\Delta\lambda$ is an important issue, the vibrating crystal offers the unique opportunity to tune intensity against bandwidth and to adjust readily the compromise between resolution and intensity without changing the crystal.

References

[1] G.E. Bacon, R.D. Lowde, Acta Crystallogr. 1 (1948) 303.
[2] C.G. Darwin, Philos. Mag. 27 (1914) 315, 675.
[3] F. Rustichelli, Neutron Inelastic Scattering, International Atomic Energy Agency, Wien, 1972.
[4] K.-D. Liß, A. Magerl, Nucl. Instr. and Meth. A 338 (1994) 90.
[5] B. Buras, T. Giebultowicz, W. Minor, A. Rajca, Phys. Status Solidi A 9 (1972) 432.
[6] K.H. Hellwege, A.M. Hellwege (Eds.), Landoldt-Börnstein, Handbuch der Physik, vol. 11, New Series III/11, Springer, Berlin, 1979.
[7] W.P. Mason (Ed.), Physical acoustics, Principles and Methods vol III, Part B, Academic Press, New York, 1965.
[8] See, H. Blank and B. Maier (Eds.), Yellow Book: Guide to Neutron Research Facilities at the ILL, Grenoble, 1988.
[9] J.W.M. DuMond, Phys. Rev. 52 (1937) 872.
[10] H. Rauch, D. Petrascheck, Dynamical neutron diffraction and its application, in: Neutron Diffraction, H. Dachs (Ed.), Springer, Berlin, 1976.
[11] A.D. Stoica, M. Popovici, J. Appl. Crystal 17 (1984) 315.
[12] A. Remhof, unpublished.
[13] B. Alefeld, Z. Physik 228 (1969) 454.
[14] A. Magerl, K.-D. Liß, C. Doll, R. Madar, E. Streichele, Nucl. Instr. and Meth. A 338 (1994) 83.
[15] R. Hock, T. Vogt, J. Kulda, Z. Mursic, H. Fuess, A. Magerl, Z. Phys. B 90 (1993) 143.
[16] This issue is studied in ongoing experiments.